International Journal of Applied Pharmaceutics

ISSN- 0975-7058 Vol 15, Issue 6, 2023

Original Article

MOLECULAR DOCKING AND DYNAMIC SIMULATION-BASED SCREENING IDENTIFIES INHIBITORS OF TARGETED SARS-COV-2 3CLPRO AND HUMAN ACE2

SARVESH GALGALE[1*], RIDA ZAINAB[2], PRADEEP KUMAR A.[3], NITHYA M.[3], SUSHA D.[1], SAMEER SHARMA[1]

[1]Department of Bioinformatics, Bangalore, BioNome, India. [2]Department of Biotechnology, Lahore College for Women University, Pakistan. [3]K. S. Rangasamy College of Technology, Thiruchengode, India
[*]Corresponding author: Sarvesh Galgale; Email: sameer21.97@gmail.com

Received: 06 Jul 2023, Revised and Accepted: 23 Aug 2023

ABSTRACT

Objective: Several genetic variations of Severe Acute Respiratory Syndrome coronavirus-2 (SARS-CoV-2) are continuously arising due to the uncontrolled dissemination of the virus during the pandemic. Omicron (B.1.1.529), the most prevalent variation of concern, has demonstrated extraordinary proliferation and pathogenicity and has emerged as the dominant variant as it has inflicted mass casualties worldwide.

Methods: Impeding the expression of 3CLpro, a coronavirus protease that is essential for digesting the RNA polyproteins, and the human angiotensin-converting enzyme 2 (ACE2) that serves as a receptor for the viral protein is identified as a competent therapeutic target. In the current study, human ACE2 and the viral 3CLpro complex was the target for the designing of novel drugs against the lethal virus. The docked complex was validated by Procheck, and the covid ligand library was investigated for its pharmacological efficacy using admetSAR 2.0. The molecular docking study was performed with the screened compounds obtained from the PubChem database against the docked protein complex.

Results: The ACE2 and 3CLpro proteins were docked together and the best docked complex was utilized for the analysis of the 1,87,419 compounds retreived from the PubChem COVID library, 18,642 compunds fulfilled the pharmacological screening and were appraised for docking with ACE2-3CLpro complex. The molecular docking results presented that the compounds 1-(4-fluorophenyl)-N'-(4-methylphenyl)propane-1,3-diamine (CID: 10038137) demonstrated significantly better binding (-18.7 kacl/mol) with favourable pharmacological properties and was therefore subjected to molecular dynamic simulations using Desmond Schrodinger 2019.2 GPU enabled package for 100 ns trajectory. The complex structure was observed to be stable after 15 ns and the average RMSD was observed to be ~0.65 nm. The complete binding energy of the complex with respect to MD simulation was-134.998+/-18.435 kj/mol which exposed that the inhibitor has a higher affinity towards the 3Clpro-ACE2 complex.

Conclusion: Consequently, this compound can be used to develop anti-covid medications to combat complications associated with Omicron infection.

Keywords: Omicron, COVID-19, SARS-CoV-2, ACE2, 3CLpro, MD simulation, Covid therapeutics

DOI: https://dx.doi.org/10.22159/ijap.2023v15i6.48782. Journal homepage: https://innovareacademics.in/journals/index.php/ijap

INTRODUCTION

Over the past years, rapidly evolving viral epidemics are posing a significant threat to global public health [1]. Numerous viral contagions, comprising of the H1N1 swine flu outbreak [2], the Ebola virus pandemic in West Africa [3], Zika virus [4], Acute Respiratory Distress Syndrome (ARDS), the Middle East Respiratory Syndrome (MERS) [5], and Severe Acute Respiratory Syndrome Corona Virus-2 (SARS-CoV-2), have been ascertained in the recent two decades [6]. The contemporaneous pestilence of coronavirus (CoV) imperils the respiratory system, cardiac tissues, hepatic cells, and renal cells, and ultimately concludes in multiple organ dysfunction (MOD). SARS-CoV-2 is constantly developing, and many variants have been identified and categorized. An early prototype of SARS-CoV-2 with a D614G mutation in the spike glycoprotein was discovered, and it was accompanied by a high transmission capacity that accelerated the global pandemic [6]. Presently, five major variants of concern have been recognized: Alpha (B.1.1.7), Beta (B.1.351), Gamma (P.1), Delta (B.1.617.2), and Omicron (B.1.1.529), which are linked to increased pathogenicity and dissemination [7, 8]. These characteristics are attributed to the propensity of the virus to evade the host immune system and promotes virus–host associations that encourage viral growth and development [9]. Following the Omicron variant, three sub-lineages have been reported as BA.1, BA.2, and BA.3, with BA.1 experiencing the highest global dispersion to date [10, 11].

The replication of the Corona Virus (CoV) begins with the attachment to the host Angiotensin Converting Enzyme-2 (ACE2) through receptor-mediated endocytosis, followed by penetration into the host cells, genomic replication, components assembly, virion formation, and its release. The S proteins from the Omicron bind to host ACE2 and invade the cell through the action of TMPRSS211 serine protease. The CoV protease 3CLpro (non-structural protein 5) is indispensable for viral RNA polyprotein cleavage and virus replication [12]. The dimeric structure of the 3CLpro proteins is biologically active, while its monomers are inactive. The N-terminal amino group, positioned between domains II and III of one monomer and the second domain of the other monomer, is conjectured to execute a significant role in protein dimerization and the development of the catalytic site of 3CLpro [12-14]. As the host ACE2 and viral S protein interaction demonstrate greater affinity, the accreditation of the viral protein and ACE2 interactions is very constructive [15, 16]. The virus exploits ACE2 to penetrate the host cell and represses its expression, which accelerates the pathogenesis of severe respiratory syndrome. ACE2 is associated with several key processes including intestinal protein breakdown, the Renin-Angiotensin System (RAS) blood pressure modulation, and vasodilation. It has been suggested that ACE2 receptor deterioration during SARS-CoV-2 infection affects its capability to defend against inflammatory responses via the RAS and bradykinin pathways [17-19]. Angiotensinogen (ANG), angiotensin 1 and 2, renin, and angiotensin converting enzyme (ACE) are the components of the RAS system. ACE2 also governs the activation of multiple inflammatory cytokines in macrophages, whereas, its down regulation promotes macrophage overexpression in CoV [20].

The 3CLpro is imperative in viral maturation while ACE2 serves as a receptor for viral glycoprotein. Therefore, elucidating the interaction between the viral and host protein will furnish greater insights into viral pathogenesis. Conventional drug development protocols can take years and cost billions to introduce novel therapeutics to the market whereas, *in silico* drug designing is quick, efficient, and cost-effective to generate novel medications. Furthermore, a number of previous research has underlined the engagement of bioactive substances with SARS-CoV-2 proteins in combating the COVID-19 outbreak, which has inspired us to undertake the present research. In the current study, the COVID-19 library (https://pubchem.ncbi.nlm.nih.gov/#query=covid-19) from the

PubChem database to screen for the potent anti-covid molecules was utilized that can effectively address the 3CLpro-ACE2 complex to minimize the detrimental effects of ACE2 down regulation. The data and conclusions established from these docking and simulations studies have assisted in the identification of safe and effective ligands that could be ordained to develop novel anti-covid drugs.

MATERIALS AND METHODS

Work station

Linux Operating system was used to perform the docking calculations and dynamic simulations in the HP Z640 workstation with 64GB RAM and Nvidia 3080Ti graphics card followed by Xeon dual processors.

Retrieval of 3D structures of the ACE2 and 3CLpro proteins

The 3-dimensional structures of the proteins, ACE2 and 3CLpro, were retrieved from the RCSB PDB (Protein Data Bank) (https://www.rcsb.org/) in. pdb format [24]. The protein structural data was constructed based on various experimentation methodologies like X-ray diffraction, NMR, electron microscopy, etc. In this study, the crystal structure of human ACE2 (PDB ID: 7U0N) was downloaded with a resolution of 2.61 Å. The antiviral protein 3CLpro (3CL-like protease) is a principal protein that potentially sunders the coronavirus polyprotein. The 3D structure of 3CLpro (PDB ID: 7WO3) was retrieved having a resolution of 2.01 Å.

Preparation of proteins for protein-protein docking

The 3D crystal structures of the proteins, ACE2 and 3CLpro, were purified preceding docking by using DS Discovery Studio (BIOVIA Discovery Studio-BIOVIA-Dassault Systèmes® (3ds.com)) to prepare both the proteins for docking. The free energy of the water molecules does not concomitant the crystallographic domiciliation. Therefore, the water molecules and the prebound ligands were removed from the crystal structures to avoid any alteration to the docking scores and to facilitate the binding with the ligands that were chosen for the study, respectively. To avoid the complexity of the protein structures, additional chains were removed from the protein structures while the A chain was retained for the analysis. The purified structures were optimized by the addition of polar hydrogen atoms [25] and validated using PROCHECK (PROCHECK home page (ebi.ac.uk)) [26] to generate the Ramachandran plot [27] and to evaluate the steric clashes and structure reliability.

Protein-protein docking of ACE2 and 3CLpro proteins

The cellular function and interactions between the ACE2 and 3CLpro proteins were evaluated through protein-protein docking using ClusPro 2.0 (https://cluspro.org/help.php) [28]. The ligands were rotated with 70,000 rotations and translated on the grid. All rotations were scored and the 1000 rotations with the least scores were selected for RMSD clustering. The 30 best models were screened after clustering and the charm minimization to eliminate steric clashes was done. Among the top 10 models, the model corresponding to Cluster 0 was downloaded from the balanced category with respect to the lowest energy and weighted score. The docked 3CLpro–ACE2 protein complex was used for further analysis [29].

Collection of the ligand library

PubChem (https://pubchem.ncbi.nlm.nih.gov) is a database of chemical compounds that proffer particulars about their physiochemical properties, bioactivities, toxicity, etc. The substance, bioassay, and compound databases are concatenated with the PubChem database [21]. The Substance repository [22] incorporates chemical characterization of the small molecules. The Compound database [22] is the depot for chemical architecture generated from the Substance database while the data about the physiological and biochemical activity of the small molecules are stored in the BioAssay database [23]. In the current study, a library of 1,87,419 compounds was constructed from the PubChem database.

Pre-processing and virtual screening of the ligand library

The COVID library retrieved from PubChem entailed 1,87,419 compounds. These compounds were filtered based on physicochemical properties, the Lipinski rule of five [30], and toxicity parameters. The pre-processing filters necessitated the removal of small molecules with disagreeable physicochemical properties and toxicity values. The pre-processing was effectuated using the ChemBioServer 2.0 web tool (https://chembioserver.vi-seem.eu/) [31]. The library was initially processed using the Chemmine R package and its physicochemical properties were analyzed. The processed data were screened according to the Lipinski Rule of Five, Partition coefficient values (log P), Polar surface area (PSA), and other chemical properties [32]. The unwanted chemical structures and moieties were eliminated after filtering and 92,547 compounds were proceeded for further analysis. The advanced filtering section was utilized to implement toxicity screening which eliminated the toxic and carcinogenic structures from the processed library. The vdW screening enabled the removal of small molecules with steric clashes. In total, 18,642 compounds fulfilled the evaluation parameters and were appraised for molecular docking studies [31, 32]. The virtual screening of the pre-processed ligand library was achieved through PyRx (https://pyrx.sourceforge.io/) [33] to attain hit compounds with advantageous biological properties towards the docked protein complex of 3CLpro and ACE2. It took around 33-36 h to complete the virtual screening of the 18,642 compounds library. The pharmacokinetic properties of the top 10 covid library compounds were further examined with admetSAR 2.0 (http://lmmd.ecust.edu.cn/admetsar2/) [34].

Preparation of the ligands

The ligand library was uploaded in Structure Data Files (SDF) format using the Open Babel section in the navigation panel. SDF corresponds to flat chemical structures as multiple structures are compressed within a single file. The ligand preparation was achieved by energy minimization and the elimination of salts from the imported SDF files using the Open Babel tools [36]. Therefore, energy minimization was executed to attain proper 3-Dimensional structures with definite bond lengths. The energy minimized values indicate the universal force field values (_uff) effectuated by the Open Babel package. These values are representative of the change implemented to the ligand moieties. Following energy minimization, the ligands were converted to PDBQT format.

Molecular docking of the ligands with the 3CLpro–ACE2 protein complex

The PyRx software integrates AutoDock 4 and AutoDock Vina to accomplish docking. The AutoDock tools package [35] integrated with PyRx aids in the preparation of the input files. The Visualization ToolKit (VTK) [37] enabled the visualization of the docked structures within the PyRx interface whereas the matplotlib was beneficial in generating the 2D plots for the ligands and the target.

The docking by PyRx assumes the 3D structures of the macromolecules as rigid that were converted to AutoDock PDBQT format for further analysis. The flexibility of the ligand by default has accounted for 9 conformational changes with different binding energies. The grid was generated and the prepared compounds were proceeded for docking. The docking results were downloaded as CSV files and analyzed with respect to binding affinity. The negative binding affinity stipulated that the ligands bind to the 3CLpro–ACE2 protein complex. The more negative the binding affinity, the better the binding [33].

MD simulation using desmond package

The MD (Molecular Dynamic) simulation was performed on the compounds with the lowest binding affinity and best physicochemical parameters. The significant hydrogen bond associations can be uncovered using simulation studies [38]. The docking calculation was further subjected to Desmond Schrodinger package 2019.2. The built-docked complex system was based on thermos dynamic stability using an OPLS force field (Optimized Potentials for Liquid Simulations) to mimic the water molecules employing the SPC (Simple Point Charge) water model. The repeating units were considered at a 10 Å distance and defined within the orthorhombic periodic boundary positions. NPT (Constant Number of atoms, Volume, and Temperature) ensemble

was used within the radius of the periodic boundary at 310K temperature and 1 Bar pressure. This was processed for 100 ns NPT formation simulation with specific frame intervals [39].

Normal mode analysis

Normal Mode Analysis (NMA) is a computer-based simulation approach for evaluating the movement patterns of atoms or molecules [40]. The NMA in this research was performed using the iMODS server (https://imods.iqfr.csic.es/). The iMODS server aids in the exploration of macromolecule functioning and generates readily accessible data on pathways that may be linked to the macromolecule in question or homologous structures.

NMA delivers better discernment about the allosteric and transition pathways associated with the biomolecules. The ICS (Internal Coordinate Space) algorithm was implemented to execute NMA wherein, the dihedral angles were considered as the variables [41, 42]. In the ICS approach, the harmonic equivalence was expanded and the number of variables was decreased which simultaneously reduced the number of modes that accorded to the conformational changes. With an increase in amplitude, the deviation from the initial structures was studied and the corresponding RMSD values were noted. From the pool of models, the model resembling the native structure was selected while refining the models.

RESULTS

Molecular docking analysis between phytochemicals and the 3CLpro-ACE2 complex

Experimental studies have exposed that the Omicron virus enters the host cell when its viral protease, 3CLpro, binds directly to the cell surface of the host's ACE2 binding receptor. This interaction enables the viral entry and initiates its replication process. In the current study, 2 major proteins (3CLpro and ACE2) were docked together (fig. 1) to investigate the binding affinity of phytochemicals against the complex.

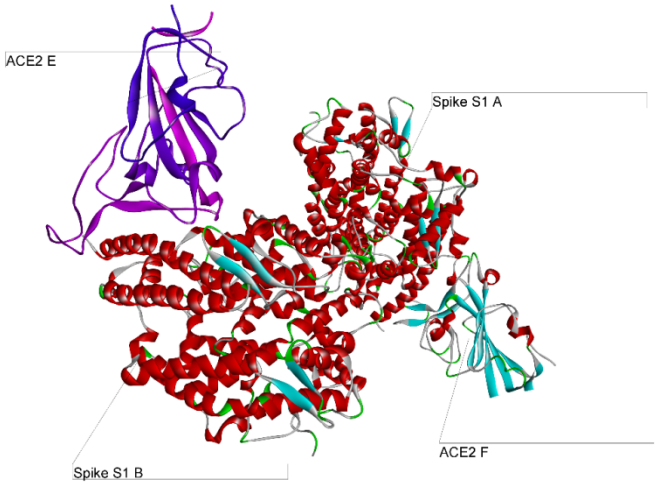

Fig. 1: 3CLpro and ACE2 docked protein-protein complex structure

All the covid library compounds were docked in contrast to the target complex and ranked based on their binding score or dock score. All the compounds which possessed binding less than-8.0 kcal/mol, were considered representative drug candidates for Omicron infection. A total of 10 compounds were selected based on the binding interactions with the 3CLpro-ACE2 docked protein complex (table 1). Out of the 10 compounds, *1-(4-fluorophenyl)-N'-(4-methylphenyl)propane-1,3-diamine* exhibited the best-docked score (-18.7 kcal/mol) with complex structure and was subjected to molecular dynamic studies to analyze the stability and binding free energies.

Table 1: Interaction of amino acid residues of 3CLpro and ACE2 complex with ligands on the receptor surface

Ligands	Binding affinity (kcal/mol)	Hydrogen bonding interactions	Hydrophobic interactions	Electrostatic interactions
10038137	-18.7	GLU A: 406, THR A: 445	GLU A: 406	GLU A: 406
10036216	-16.3	GLN A: 442, THR A: 445	THR A: 445, ASP A: 132	THR A: 445
10061134	-16.1	GLN A: 552	--	--
10017	-13.5	HIS A: 162, TYR A: 160, SER A: 174, LEU A: 30, GLY A: 145	TYR A: 160, LEU A: 30	LEU A: 30
10036127	-12.8	--	--	--
10019	-12.3	GLY A: 145, SER A: 146, TYR A: 160, PRO A: 147, HIS A: 162	SER A: 146, TYR A: 160, PRO A: 147	TYR A: 160, PRO A: 147
10218299	-11.9	ARG A: 393, PHE A: 390, THR A: 347, ASP A: 350, TYR A: 385, ASN A: 394	THR A: 347, ASP A: 350,	THR A: 347, ASP A: 350, TYR A: 385
10166	-10.4	ASP A: 350	--	--
10112	-10.2	--	--	--
10216432	-10.1	TYR A: 385, HIS A: 401	HIS A: 401, GLU A: 145	HIS A: 401

3D structure validation of ACE2 and 3CLpro by ramachandran plot

The proteins ACE2 and 3CLpro, PDB IDs: 7U0N and 7WO3 respectively, were examined for their 3D protein structures and steric hindrance. The purified structure of 7U0N (ACE2) contained 597 amino acids (3 sheets, 2 beta hairpins, 1 beta bulge, 6 strands, 31 helices, 58 helix-helix interacts, 37 beta turns, 6 gamma turns, and 3 disulfides). The purified structure of 7WO3 had 290 amino acids (3 sheets, 7 beta hairpins, 6 beta bulges, 14 strands, 10 helices, 7 helix-helix interacts, 24 beta turns, and 2 gamma turns) (fig. 2).

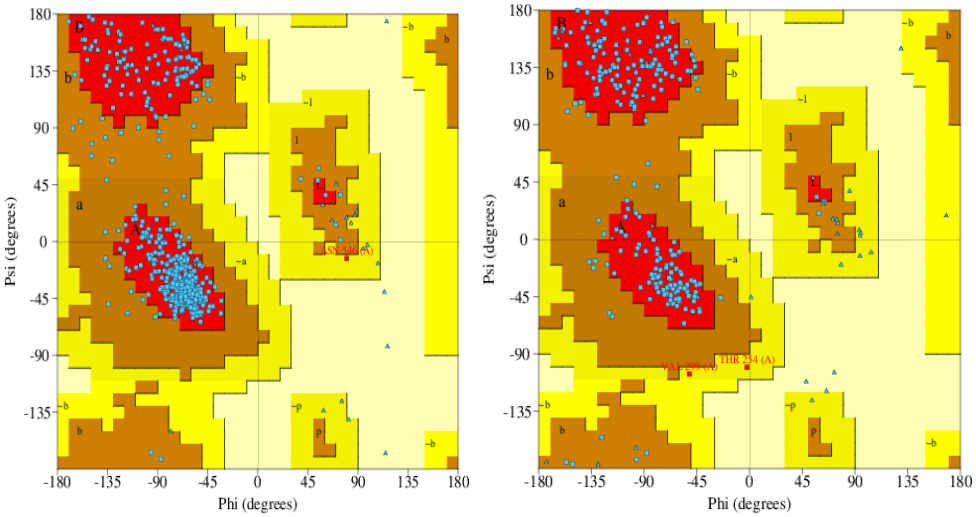

a. ACE2 **bs. 3CLpro**

Fig. 2: Ramachandran plots of purified ACE2 and 3CLpro proteins

The Ramachandran plot revealed that the ACE2 protein has 491 residues in the most favored region, 44 residues in additionally allowed regions, one residue in the generously allowed region, and no residues in the disallowed region. The purified structure of ACE2 has 32 glycine and 27 proline residues. Whereas, the 3CLpro protein has 193 residues in the most favored region, 33 residues in additionally allowed regions, two residues in the generously allowed region, and no residues in the disallowed region. The purified structure of 3CLpro has 35 glycine and 5 proline residues (fig. 2).

Molecular interaction studies of the top 3 best compounds

The docking interactions were analyzed to ascertain the dominant interactions in the binding pocket of the protein. The hydrophobicity of the protein binding pocket is vital in determining the protein topology and stability as it helps to eliminate unwanted interactions with the non-structural water molecules. Good hydrophobicity was observed on the protein surface. It was noticed that the ligand 10038137 was interacting with GLU 406 and THR 445 by establishing hydrogen bonds (fig. 3). While the ligand 10036216 was majorly interacting with GLN 442 and THR 445 by establishing hydrogen bonds in the binding pocket of the protein (fig. 4). Similarly, the ligand 10061134 has established five hydrogen bonds with amino acids THRC347, ASP 350, TYR 385, ARG 393, and ASN 394 respectively (fig. 5).

Drug likeness of the selected top 10 compounds

The physicochemical properties of the selected 10 compounds were studied on the ChemBioServer 2.0. All the selected compounds were plant-based, and some of them obeyed Lipinski's rule of five (table 2).

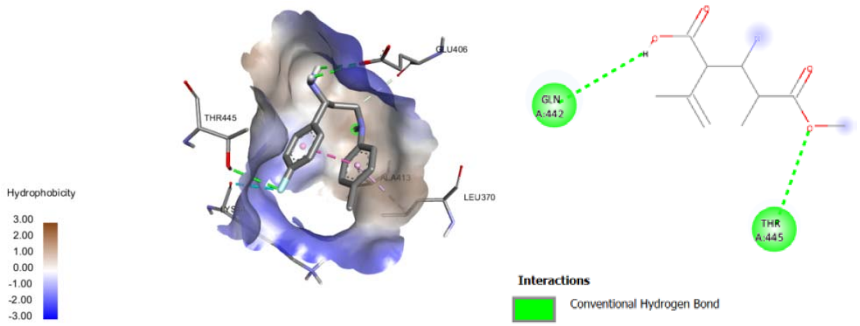

Fig. 3: 3D and 2D interactions of 10038137 with 3CLpro-ACE2 complex

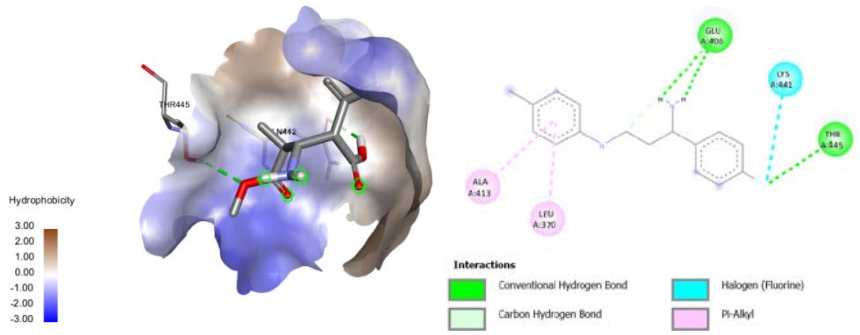

Fig. 4: 3D and 2D interactions of 10036216 with 3CLpro-ACE2 complex

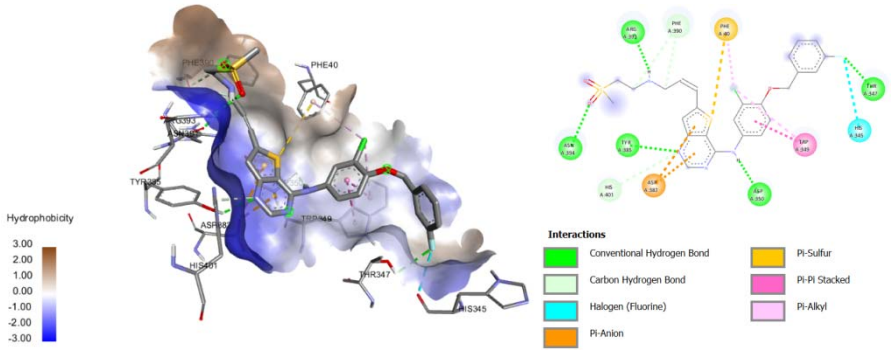

Fig. 5: 3D and 2D interactions of 10061134 with 3CLpro-ACE2 complex

Table 2: Physicochemical and drug-likeness properties of the active compounds

PubChem ID	Molecular name	MW	Logp	HBA	HBD	TPSA	Violation	AMR
10038137	1-(4-fluorophenyl)-N'-(4-methylphenyl)propane-1,3-diamine	258.150	3.194	2	3	38.050	Accepted	77.48
10036216	(2S,3R,4R)-3-amino-5-methoxy-4-methyl-5-oxo-2-prop-1-en-2-ylpentanoic acid	215.120	0.067	5	3	89.620	Accepted	55.47
10061134	2-(2,6-dichloro-4-hydroxyanilino)-1,4-dihydroimidazol-5-one	258.990	1.997	5	4	84.400	Accepted	69.22
10017	2-fluoroethyl carbonochloridate	125.990	0.598	2	0	26.300	Accepted	23.06
10036127	5-bromo-3H-1-benzofuran-2-one	211.950	3.159	2	1	33.370	Accepted	43.69
10019	3-fluoropropan-1-amine	77.060	-0.087	1	2	26.020	Accepted	19.29
10218299	N-[3-chloro-4-[(3-fluorophenyl)methoxy]phenyl]-6-[3-(2-methylsulfonylethylamino)prop-1-ynyl]thieno[3,2-d]pyrimidin-4-amine	544.080	3.923	7	2	96.440	1 violation	141.83
10166	(1R,3S)-9-methoxy-1,3-dimethyl-3,4-dihydro-1H-benzo[g]isochromene-5,10-dione	272.100	3.497	4	2	58.920	Accepted	73.74
10112	Aragonite	59.990	-2.697	3	0	63.190	Accepted	6.77
10216432	2-(3-acetamidophenyl)-N-[[(2S)-4-[(3,4-difluorophenyl)methyl]morpholin-2-yl]methyl]acetamide	417.190	1.792	6	2	70.670	Accepted	112.56

MW: Molecular Weight; HBA: Hydrogen bond acceptor; HBD: Hydrogen bond donor; TPSA: topological polar surface area; AMR: Atom Molar Refractivity; Accepted: Indicates that the drug follows all the five rules of Lipinski.

ADMET analysis using admetSAR 2.0

All the ADMET biological properties of covid library compounds were assessed using admetSAR 2.0. All the compounds showed significant human intestinal absorption and blood-brain barrier infiltration. None of the compounds observed any carcinogenic properties in their nature followed by a negative AMES test which can be seen in table 3.

Table 3: Pharmacokinetic studies using admetSAR web server

Ligand	Human intestinal absorption	Caco-2	Blood-brain barrier	Human oral bioavailability	MATE-1	AMES mutagen city	Acute oral toxicity
10038137	0.9856	0.5589	0.9913	0.9	0.88	0.55	1.985
10036216	0.9666	0.7329	0.9497	0.5714	0.98	0.74	2.789
10061134	0.9807	0.8599	0.9805	0.6857	0.66	0.76	1.559
10017	0.9593	0.5671	0.9936	0.5286	0.98	0.6100	4.512
10036127	0.9727	0.8968	0.908	0.5714	0.5714	0.5714	0.5714
10019	0.9197	0.8027	0.9968	0.8857	1.00	0.85	3.316
10218299	0.9583	0.8133	0.974	0.7143	0.78	0.52	2.122
10166	0.9956	0.7583	0.2616	0.6714	0.96	0.96	0.96
10112	0.8126	0.6085	0.9914	0.9914	1.00	0.72	1.053
10216432	0.9744	0.7984	0.9878	0.5286	0.96	0.5	1.836

Molecular dynamic simulation of the best compound

Using the docked calculations, the (PubChem CID: 10038137) compound was subjected to Molecular Dynamic Simulation using Desmond Schrodinger 2019.2 GPU enabled package which indulges the stability of protein and provides insight with respect to simulation was equilibrated. The docked complex was pre-processed to identify and repair the missing residues. The complex was then prepared for simulation by applying OPLS force for 100 ns to analyze the stability and interactions.

The complex structure of the RMSD plot was shown in fig. 2. RMSD was performed and plotted for 3CLpro and ACE2 complex which were modulated during the 100 ns MD simulation. The complex structure was observed to be stable after 15 ns which can be seen in fig. 2. The average values of the ACE2-3CLpro complex were ~0.65 nm for 100 ns simulation which indicates the protein complex to be stable during the MD simulation.

RMSF (Root Mean Square Fluctuation) analysis was performed with the close and open conformation of the protein. Initial and final

conformations of the dynamics were analyzed using the PyMol software.

Binding free energy (MM/GBSA) of the protein complex

The complete binding energy of the complex with respect to MD simulation was-134.998+/-18.435 kj/mol which exposed that the inhibitor has a higher affinity towards the 3Clpro-ACE2 complex.

A detailed representation of the protein-ligand interaction is depicted in fig. 6. The interaction diagram specifically depicts those interactions which were predominantly observed for at least more than 30% of the simulation time (100 ns). For the given complex the ligand has established significant interactions with the amino acids like ARG, ASP, ALA, VAL, and PRO.

The interactions of the protein and ligand are further assessed by the type of bond they establish. The protein's ligand contacts represent the interaction type. The ligands have interacted with the proteins through hydrogen bonds (green), water bridges (blue), and hydrophobic interactions (purple) as depicted in fig. 7. The stacked bar charts representing values greater than 1.0 indicates that the protein residues may make multiple contacts of the same subtype with the ligand.

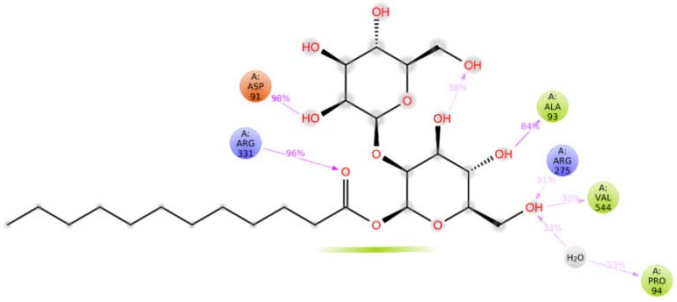

Fig. 6: Bond interaction of ligands with amino acid residues, Negative charged (Orange), Hydrophobic (Green), Solvent exposure (Grey background), Charged positive (Purple), Water (Grey)

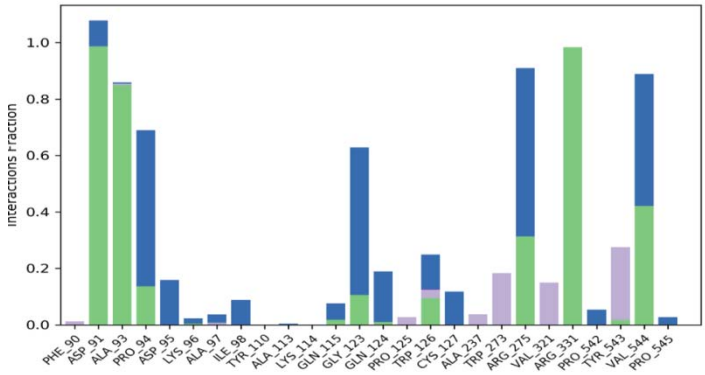

Fig. 7: Protein-ligand contacts, ASP_91, ALA_93, ARG_331, ARG_275, and VAL_544 showed the highest contact with H-bonds (Green), Hydrophobic interactions (purple), and water bridges (Dark blue)

The Protein RMSD graph provides information on the structural conformation of the protein throughout the simulation, while the ligand RMSD represents the stability of the ligand with respect to the protein and its binding pocket (fig. 8). The ligand RMSD values are significantly lower than the protein RMSD values, and these values indicate that the ligand has not diffused away from its initial binding site.

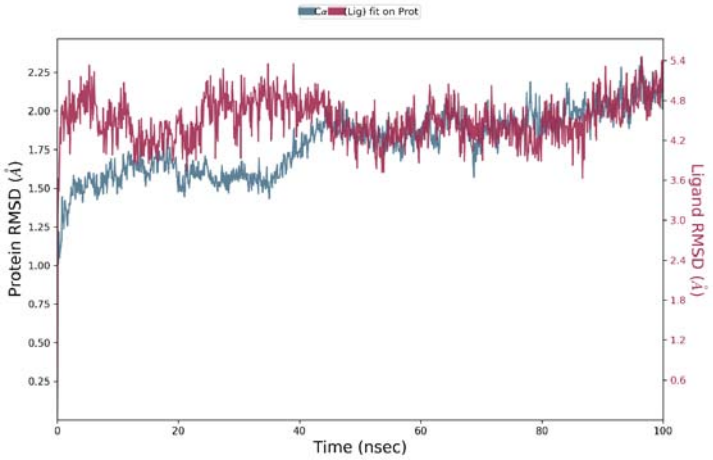

Fig. 8: Protein-ligand RMSD graph, the RMSD evolution of the protein is depicted along Y-axis (left) and the ligand is represented along Y-axis (right)

The Root Mean Square Deviation (RMSD) (fig. 9) is used to measure the average change in displacement of a selection of atoms for a particular frame with respect to a reference frame. From the RMSD graph, it is evident that the ACE2-3CLPro-10038137 complex had lower RMSD as compared to ACE2-3CLPro and 10038137 individually. Furthermore, it was noticed that the ACE2-3CLPro complex was stabilizing with 10038137 ligands during the period. It was observed that the protein and ligand started to stabilize from approximately 40 ns and remained stable throughout the simulation without major fluctuations.

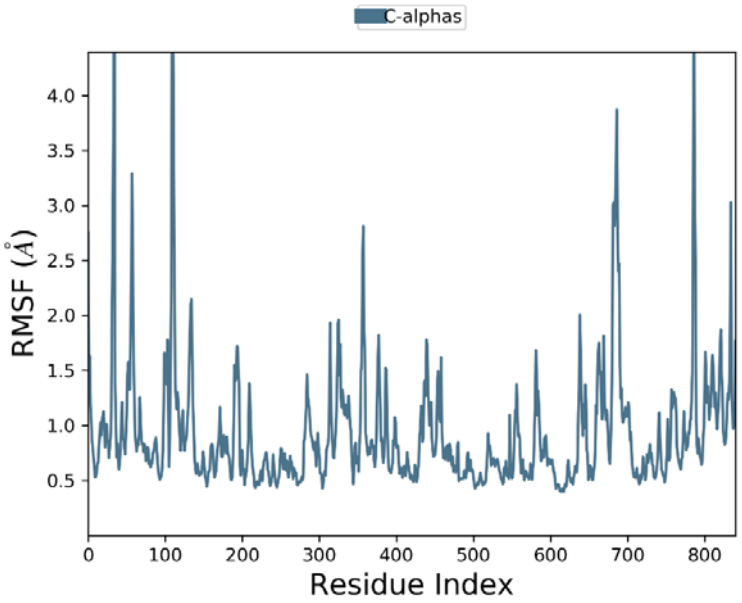

Fig. 9: Protein RMSF, the peaks in the graphs indicate the area of the protein that fluctuates most during simulation. The N-and C-terminal fluctuate the highest whereas the secondary structures fluctuate the least

Root Mean Square Fluctuation (RMSF) (fig. 9) represents residual changes and the regions that highly fluctuate during the simulation showed the characterizing of local changes along the protein chain. As the ACE2-3CLPro complex had a significant number of secondary structure elements like loops and bulges, few fluctuations were observed in the protein complex.

Six parameters are employed to evaluate the properties of the ligand (fig. 10). The PSA (Polar Surface Area) analyzes the solvent-accessible area in a molecule contributed by Oxygen and nitrogen atoms. While the SASA (Solvent Accessible Surface Area) estimates the surface area of a molecule accessible by a water molecule. The MolSA (Molecular Surface Area) is equivalent to van der Waals's surface area. The radius of gyration (rGyr) is the measure of ligand extendedness and the ligand RMSD is the measure of the deviation of the ligand with respect to the reference conformation. Intramolecular Hydrogen Bonds (intraHB) represent the number of internal hydrogen bonds within a ligand molecule.

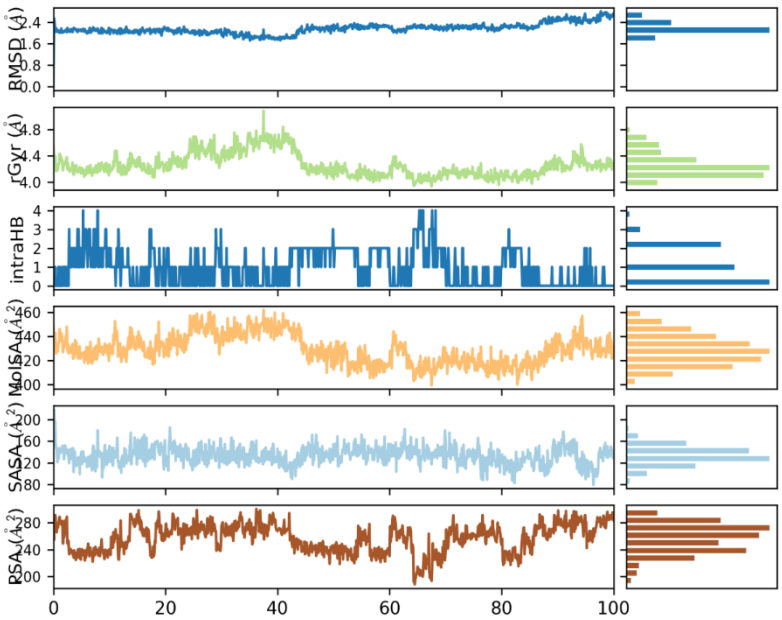

Fig. 10: Ligand properties, the ligand properties are evaluated across six parameters: Ligand RMSD, radius of gyration, intramolecular hydrogen bonds, molecular surface area, solvent accessible surface area, and polar surface area

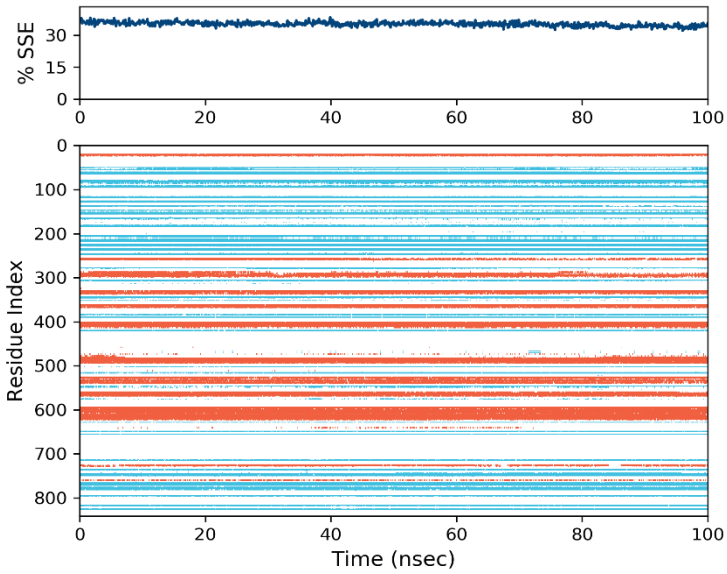

Fig. 11: Protein secondary structure, in the plot, alpha helices are represented by orange lines while the beta-strands are represented by blue lines

Protein secondary structures like alpha-helices and beta-strands are monitored throughout the simulation. The plot %SSE summarizes the SSE composition for each trajectory frame throughout the simulation, and the plot at the bottom monitors each residue and its SSE assignment over time (fig. 11).

Normal mode analysis

Normal Mode simulation has been performed using iMODs (fig. 12) webserver to analyze the atom index (fig. 13), B-factor, Eigenvalues, and elasticity of the protein with respect to ligand complexity. 3CLpro and ACE2 complex has very good unwinding elasticity followed by co-variance with eigenvalue = 2.630496e-05, respectively.

The normal mode analysis helps determine the degree of mobility of the protein structures. The deformability, B-factor, Eigenvalues, Variance, and residue index parameters determine the potential of the molecule to deform each residue. The B-Factor (fig. 1) describes the displacement of the atomic positions from an average mean square displacement. Higher flexibility of the macromolecules results in larger displacement, which eventually results in lower electron density. The positions of the atoms correspond to irregularities in the crystal structures. Greater B-factor values represent higher mobility and flexibility of the atoms in the crystal structure. The energy utilized to deform the protein structure is depicted by the Eigenvalues and the deformation energy is directly proportional to the motion stiffness (fig. 15). Lower eigenvalues represent a greater probability of deformation and the eigenvalues are inversely proportional to the variance-related to normal mode (fig. 16). The coupling between the residues may be related to correlated, uncorrelated, or anti-correlated motions which are represented by the covariance matrix (fig. 17). The atoms connected through springs are identified with an elastic network (fig. 18).

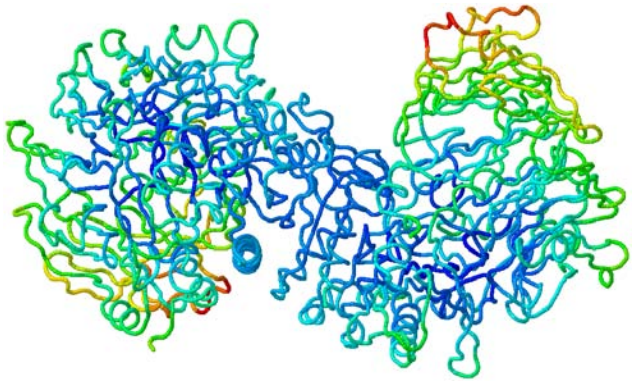

Fig. 12: Normal mode simulation obtained using iModS

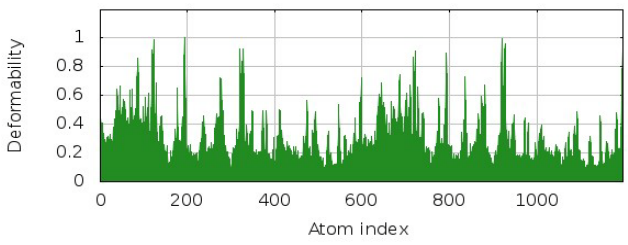

Fig. 13: Atom index at 10ns

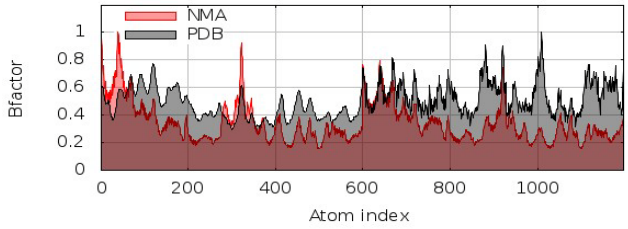

Fig. 14: B-factor or mobility, the main-chain deformability is a measure of the capability of a given molecule to deform at each of its residues

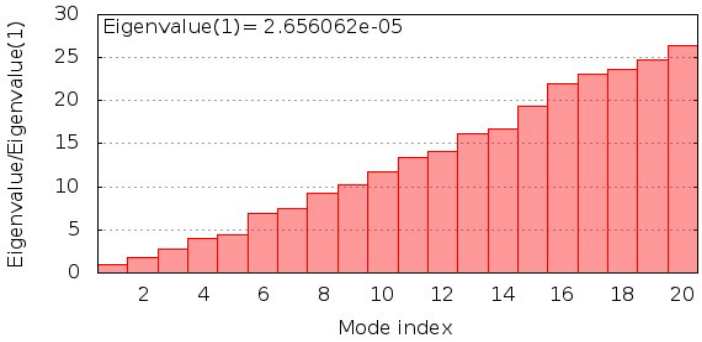

Fig. 15: Eigen values, the eigenvalue associated with each normal mode represents the motion stiffness. Its value is directly related to the energy required to deform the structure. The lower the eigenvalue, the easier the deformation

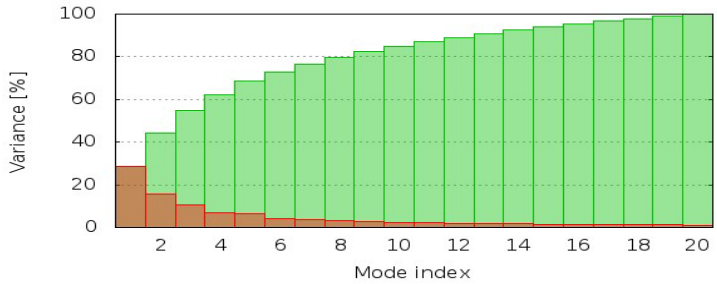

Fig. 16: Variance associated with normal mode, in the graph, the colored bars in red represent the individual variances and the green bars represent the cumulative variances

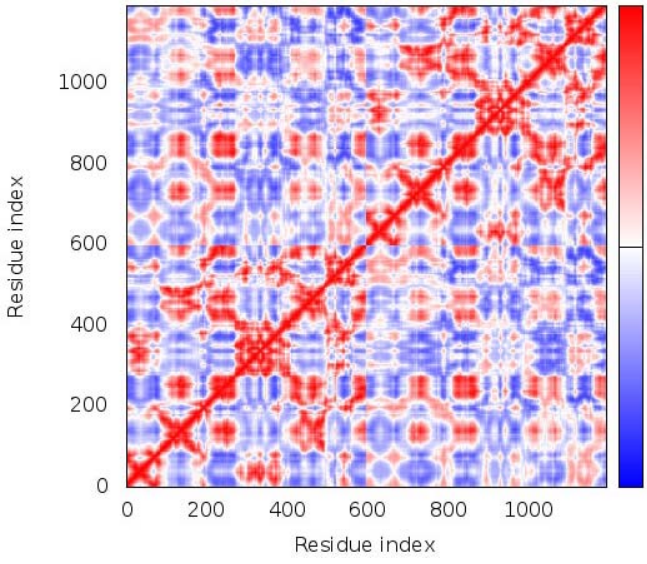

Fig. 17: Covariance map, the coupling between the pair of residues is associated with (correlated (red), uncorrelated (white), or anti-correlated (blue) motions

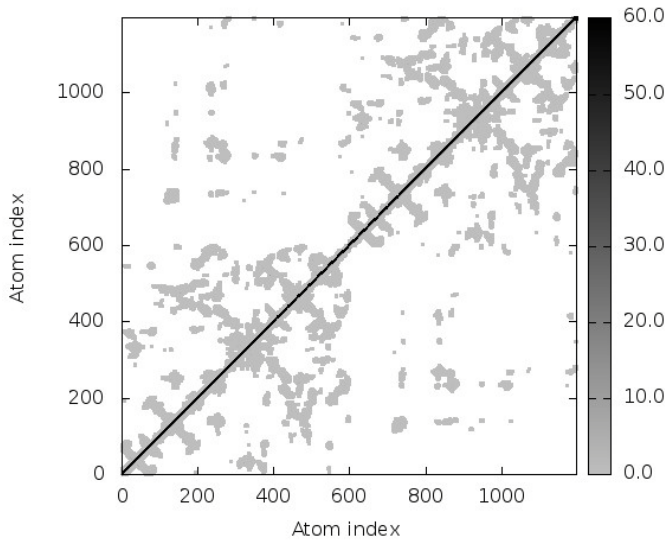

Fig. 18: Elastic network, each dot denotes one spring within the respective atoms pair. The dots are colored based on the stiffness where the dark grey dots indicate the stiffer springs and vice versa

DISCUSSION

The Omicron variant marks the start of a new phase of the COVID-19 outbreak. The novel Omicron strain with increased infectivity was initially discovered in South Africa in November 2021 [6]. Additional research indicates that the Omicron variant did not evolve from the previously identified variants, as indicated by various discrepancies in their genomic composition. They could be the result of silent evolution in a population with limited sequencing, long-term evolution in one or a few individuals with chronic infection, or evolution in other species, particularly rodents [11]. In contrast to previous SARS-CoV-2 strains, which primarily infiltrate the pulmonary organs and produce fatal sickness, the Omicron strain predominantly affects the respiratory system and induces milder symptoms [8]. SARS-receptor-binding CoV's domain interacts with human ACE2, which is present in pharyngeal surface cells and lung epithelial cells. This binding causes a fusion of the human S protein with the human cell membrane, culminating in genetic material duplication with the host cells. Omicron BA.1 features 37 amino acid alterations in the virus's spike (S) protein, fifteen of which are in the receptor binding domain. A vast number of changes was observed in the RBD of Omicron BA.1, particularly N501Y, resulting in stronger ACE2 adherence than the archetypal RBD of the Wuhan strain [8, 10]. Owing to its infectivity and vaccine-escape modifications, the Omicron strain has generated immense concern among the clinical community. Currently, up to 60 mutations in the BA.1 lineage and 52 mutations in the BA. 2 lineage have been documented [8, 11].

The most primordial step in the viral transmission of SARS-CoV-2 is the viral invasion into the cell. SARS-CoV-2 embeds the spike surface glycoprotein. The S protein's RBD adheres to the receptor on the host cell and facilitates viral invasion and migration. The discharge of the spike fusion peptide, which is synthesized when the host protease cleaves the S protein, permits viral permeation [16, 17]. ACE2 is mostly concentrated in the alveolar epithelial cells and is responsible for lowering the surface tension of these cells, thereby preventing alveolar cells from collapsing. ACE2 is imperative to corroborate adequate gaseous exchange across the lungs. An impairment of these cells would culminate in significant lung injury, which was frequently reported in COVID-19 patients. The SARS-CoV-2 S protein coheres with the host ACE2, which induces viral endocytosis and diminishes ACE2 functioning. As a consequence of this interaction, the cells are deprived of ACE2 that were accountable for shielding the pulmonary cells from any damage. Accordingly, the host is more susceptible to viral invasion [18]. The terminus of ACE2's subdomain 1 is where the S protein's receptor-binding domain interacts. The host cell is activated when the viral envelope unites with the host cell membrane. Viral RNA that initiates transmission is disseminated into the cytoplasm upon confluence [16-19]. Therefore, by restricting the virus from infiltrating host cells through the ACE2 receptor, the host is sheltered against Corona Virus Disease (CoVD).

The current study focused on implementing *in silico* techniques to investigate the anti-covid library, which encompassed 1,87,419 compounds, towards SARS-CoV-2. Premised on the pharmacological characteristics, the library was pre-processed and screened. In total, 18,642 compounds satisfied the criteria for examination and were examined for molecular docking against the 3CLpro and ACE2 complex (fig. 1) through PyRx, and their binding affinities were determined (table 1). The physicochemical properties (table 2) and the pharmacological efficacy of the compounds were further evaluated to determine their drug-likeness properties. The top 3 compounds corresponding to the best docking scores were visualized (fig. 3-5).

The compound 1-(4-fluorophenyl)-N'-(4-methylphenyl) propane-1,3-diamine (PubChem CID: 10038137) exhibited the best binding affinity of-18.7 kcal/mol (table 1) against the 3CLpro-ACE2 complex. This binding displayed significant hydrogen bonding and hydrophobic and electrostatic interactions at the binding site (fig. 4 and 7). The compound 10038137 is patented as an anti-inflammatory PLA2 (Phospholipase A2) inhibitor [43]. Some of the symptoms of CoVD include hypoxia, platelet aggregation, inflammation, vessel damage, etc [44]. The PLA2 inhibitors are effective in addressing elevated platelet generation and, accumulation of platelets and vascular diseases [45]. The 5-bromobenzofuran derivatives have demonstrated antiviral properties [46]. The rapid reduction of blood oxygen levels (hypoxemia/hypoxia) and the subsequent breathing and circulation-associated symptoms are among the major symptoms of COVID-19. 3-Fluropropylamine is used to address hypoxia-induced symptoms.

The Omicron virus predominantly affects the respiratory system and provokes ARDS. The most apparent aspect of ARDS is the cytokine storm that advances with the release of cytokines. The pernicious immune response induces ARDS, pulmonary collapse, and organ damage that affects the hepatic, cardiac kidney, and central nervous system, which ultimately culminates in death. Cellular kinases can participate in the different phases of the virus's life cycle and therefore, the kinase has been proposed as potential moderators of various viral infections [20, 47]. Numerous kinases are involved in the development of CoVD-related complications, including asthma, inflammation, and fibrosis. To combat pulmonary viral infections, kinase inhibitors deploy immediate antiviral effects as well as anti-inflammatory, cytokine-suppressive, and anti-fibrotic properties, which are beneficial in the management of CoVD symptoms [48, 49]. In the present study, the compound, with PubChem CID: 10218299,

(*N*-[3-chloro-4-[(3-fluorophenyl)methoxy]phenyl]-6-[3-(2-methylsulfonylethylamino)prop-1-ynyl]thieno[3,2-d]pyrimidin-4-amine) is a thienopyrimidine compound which is a tyrosine kinase inhibitor and therefore, it can be hypothesized that this compound may be beneficial in managing the detrimental CoVD symptoms accelerated due to the cytokine release.

The compound Eleutherin (PubChem CID: 10166) is an adaptogen that assists in stress management. Additionally, this ligand has been utilized to address inflammation and diabetes and to improve cognitive functions. DNA topoisomerase 2 is the key enzyme that regulates the topology of the DNA in the viruses, which in turn determines the packing, assembly, and replication of the viruses. The compound Eleutherin is a class of DNA topoisomerase 2 inhibitors that demonstrate antiviral properties [50]. In the current study, Eleutherin has displayed better binding with the 3CLpro-ACE2 complex. Aragonite (Calcium carbonate) is a common mineral used to treat bone and nerve damage. A clinical trial was conducted to evaluate the safety, efficacy, and tolerability of Amorphous Calcium Chloride (ACC) against moderate to severe CoV patients. The patients administered with ACC displayed faster recovery than those administered with a placebo [51].

Impeding the expression of 3CLpro, a protease that is essential for digesting the polyproteins that are synthesized from RNA molecules, is one of the most well-known therapeutic targets for CoVD. A candidate protein ACE2 is a type I transmembrane metallocarboxypeptidase that is essential for the RAS network. The S protein of SARS-CoV-2, which initiates cell invasion into host cells and viral proliferation in the target tissue, is identified as a competent receptor for human ACE2. The novel targets were investigated to determine potential antiviral candidates. From the findings of molecular docking studies, it is evident that the top 10 compounds have better binding toward the complex. The top compound i.e., 1-(4-fluorophenyl)-N'-(4-methylphenyl) propane-1,3-diamine, was further assessed by molecular dynamic simulation studies to evaluate their RMSD, RMSF, Protein-Ligand contact, binding free energy, ligand properties, etc. (fig. 6-11). Though there is minimal research to corroborate the clinical significance and pharmacological relevance of the candidate. It is evident from the current study that all the top 10 ligand molecules obey the pharmacological screening parameters and are beneficial in addressing various comorbidities associated with Omicron infection. The current findings will serve as the basis for future *in vivo* and *in vitro* studies to assure the effectiveness of anti-Omicron medications.

CONCLUSION

Examining ligand binding to the 3CLpro-ACE2 complex was the objective of the current study. These compounds have superior binding interactions, structural conformations, and persistence at the binding site of the ACE2 receptor. In the current investigation, the ligand moieties 1-(4-fluorophenyl)-N'-(4-methyl phenyl) propane-1,3-diamine, 5-bromobenzofuran, ACC, Fluropropylamine, (*N*-[3-chloro-4-[(3-fluorophenyl) methoxy]phenyl]-6-[3-(2-methylsulfonylethylamino)prop-1-ynyl]thieno[3,2-d]pyrimidin-4-amine), and Eleutherin have potential properties to be developed as anti-covid drugs. The ligand 1-(4-fluorophenyl)-N'-(4-methylphenyl) propane-1,3-diamine demonstrated the best binding with the complex, in addition to favorable pharmacological properties. Therefore, this compound can be appraised to design anti-covid drugs that address Omicron-related comorbidities.

ACKNOWLEDGMENT

We thank BioNome for providing us with scientific support in the bioinformatics research project.

FUNDING

Nil

ABBREVIATIONS

MERS - The Middle East Respiratory Syndrome, SARS-CoV-2 - Severe Acute Respiratory Syndrome Corona Virus 2, CoVD - Corona Virus Disease, CoV - Corona Virus, MOD - Multiple Organ Dysfunction, ACE2 - Angiotensin-Converting Enzyme 2, RAS - Renin-Angiotensin System, ANG – Angiotensinogen, ARDS - Acute respiratory distress syndrome

AUTHORS CONTRIBUTIONS

Sarvesh Galgale, Susha D, and Sameer Sharma have performed the experimental procedures, while Rida Zainab, Pradeep Kumar A, and Nithya M have work on the research process and the review of literature.

CONFLICT OF INTERESTS

The author declares that they have no competing interests.

REFERENCES

1. Widdowson MA, Bresee JS, Jernigan DB. The global threat of animal influenza viruses of zoonotic concern: then and now. J Infect Dis. 2017;216 Suppl 4:S493-8. doi: 10.1093/infdis/jix331, PMID 28934463.
2. Klemm C, Das E, Hartmann T. Swine flu and hype: a systematic review of media dramatization of the H1N1 influenza pandemic. J Risk Res. 2016;19(1):1-20. doi: 10.1080/13669877.2014.923029.
3. Jacob ST, Crozier I, Fischer WA II, Hewlett A, Kraft CS, Vega MA de L. Ebola virus disease. Nat Rev Dis Primers. 2020;6(1). doi: 10.1038/s41572-020-0147-3.
4. Baud D, Gubler DJ, Schaub B, Lanteri MC, Musso D. An update on Zika virus infection. Lancet. 2017;390(10107):2099-109. doi: 10.1016/S0140-6736(17)31450-2, PMID 28647173.
5. Memish ZA, Perlman S, Van Kerkhove MD, Zumla A. Middle east respiratory syndrome. Lancet. 2020;395(10229):1063-77. doi: 10.1016/S0140-6736(19)33221-0.
6. Tian D, Sun Y, Xu H, Ye Q. The emergence and epidemic characteristics of the highly mutated SARS-CoV-2 omicron variant. J Med Virol. 2022;94(6):2376-83. doi: 10.1002/jmv.27643, PMID 35118687.
7. Fan Y, Li X, Zhang L, Wan S, Zhang L, Zhou F. SARS-CoV-2 omicron variant: recent progress and future perspectives. Signal Transduct Target Ther. 2022;7(1):141. doi: 10.1038/s41392-022-00997-x, PMID 35484110.
8. Shrestha LB, Foster C, Rawlinson W, Tedla N, Bull RA. Evolution of the SARS-CoV-2 omicron variants BA.1 to BA.5: implications for immune escape and transmission. Rev Med Virol. 2022;32(5):e2381. doi: 10.1002/rmv.2381, PMID 35856385.
9. Ao D, Lan T, He X, Liu J, Chen L, Baptista Hon DT. SARS-CoV-2 omicron variant: immune escape and vaccine development. Med. 2022;3(1):e126. doi: 10.1002/mco2.126, PMID 35317190.
10. Kannan S, Shaik Syed Ali P, Sheeza A. Omicron (B.1.1.529)–variant of concern-molecular profile and epidemiology: a mini review. Eur Rev Med Pharmacol Sci. 2021;25(24):8019-22. doi: 10.26355/eurrev_202112_27653, PMID 34982466.
11. Ettaboina SK, Nakkala K, Laddha KS. A mini-review on SARS-COVID-19-2 omicron variant (B.1.1.529). Sci Med J. 2021;3(4):399-406. doi: 10.28991/SciMedJ-2021-0304-10.
12. Liu Y, Liang C, Xin L, Ren X, Tian L, Ju X. The development of coronavirus 3C-like protease (3CLpro) inhibitors from 2010 to 2020. Eur J Med Chem. 2020;206:(112711). doi: 10.1016/j.ejmech.2020.112711, PMID 32810751.
13. Sisay M. 3CLpro inhibitors as a potential therapeutic option for COVID-19: available evidence and ongoing clinical trials. Pharmacol Res. 2020;156:(104779). doi: 10.1016/j.phrs.2020.104779, PMID 32247821.
14. Roe MK, Junod NA, Young AR, Beachboard DC, Stobart CC. Targeting novel structural and functional features of coronavirus protease nsp5 (3CLpro, Mpro) in the age of COVID-19. J Gen Virol. 2021;102(3). doi: 10.1099/jgv.0.001558, PMID 33507143.
15. Bhalla V, Blish CA, South AM. A historical perspective on ACE2 in the COVID-19 era. J Hum Hypertens. 2021;35(10):935-9. doi: 10.1038/s41371-020-00459-3, PMID 33318644.
16. Zhang X, Li S, Niu S. ACE2 and COVID-19 and the resulting ARDS. Postgrad Med J. 2020;96(1137):403-7. doi: 10.1136/postgradmedj-2020-137935, PMID 32522846.

17. Chaudhry F, Lavandero S, Xie X, Sabharwal B, Zheng YY, Correa A. Manipulation of ACE2 expression in COVID-19. Open Heart. 2020;7(2):e001424. doi: 10.1136/openhrt-2020-001424, PMID 33443121.
18. Jia H, Neptune E, Cui H. Targeting ACE2 for COVID-19 therapy: opportunities and challenges. Am J Respir Cell Mol Biol. 2021;64(4):416-25. doi: 10.1165/rcmb.2020-0322PS, PMID 33296619.
19. Kai H, Kai M. Interactions of coronaviruses with ACE2, angiotensin II, and RAS inhibitors-lessons from available evidence and insights into COVID-19. Hypertens Res. 2020;43(7):648-54. doi: 10.1038/s41440-020-0455-8, PMID 32341442.
20. Alexpandi R, De Mesquita JF, Pandian SK, Ravi AV. Quinolines-based SARS-CoV-2 3CLpro and RdRp inhibitors and Spike-RBD-ACE2 inhibitor for drug-repurposing against COVID-19: an *in silico* analysis. Front Microbiol. 2020;11:1796. doi: 10.3389/fmicb.2020.01796, PMID 32793181.
21. Kim S, Chen J, Cheng T, Gindulyte A, He J, He S. PubChem 2019 update: improved access to chemical data. Nucleic Acids Res. 2019;47(D1):D1102-9. doi: 10.1093/nar/gky1033, PMID 30371825.
22. Kim S, Thiessen PA, Bolton EE, Chen J, Fu G, Gindulyte A. PubChem substance and compound databases. Nucleic Acids Res. 2016;44(D1):D1202-13. doi: 10.1093/nar/gkv951, PMID 26400175.
23. Wang Y, Bryant SH, Cheng T, Wang J, Gindulyte A, Shoemaker BA. PubChem Bioassay: 2017 update. Nucleic Acids Res. 2017;45(D1):D955-63. doi: 10.1093/nar/gkw1118, PMID 27899599.
24. Burley SK, Berman HM, Kleywegt GJ, Markley JL, Nakamura H, Velankar S. Protein data bank (PDB): the single global macromolecular structure archive. Methods Mol Biol. 2017;1607:627-41. doi: 10.1007/978-1-4939-7000-1_26, PMID 28573592.
25. Jayasurya, Swathy, Susha, Sharma S. Molecular docking and investigation of Boswellia serrata phytocompounds as cancer therapeutics to target growth factor receptors: an *in silico* approach. Int J Appl Pharm. 2023;15(4):173-83. doi: 10.22159/ijap.2023v15i4.47833.
26. Laskowski RA, MacArthur MW, Thornton JM. PROCHECK: validation of protein-structure coordinates. In: International tables for crystallography. Chester, England: International Union of Crystallography; 2012. p. 684-7. doi: 10.1107/97809553602060000882.
27. Laskowski RA, Furnham N, Thornton JM. The Ramachandran plot and protein structure validation. In: Biomolecular forms and functions. Teaneck: World Scientific Publishing/Indian Institute of Science; 2013. p. 62-75.
28. Kozakov D, Hall DR, Xia B, Porter KA, Padhorny D, Yueh C. The ClusPro web server for protein-protein docking. Nat Protoc. 2017;12(2):255-78. doi: 10.1038/nprot.2016.169, PMID 28079879.
29. Comeau SR, Gatchell DW, Vajda S, Camacho CJ. ClusPro: an automated docking and discrimination method for the prediction of protein complexes. Bioinformatics. 2004;20(1):45-50. doi: 10.1093/bioinformatics/btg371, PMID 14693807.
30. Chen X, Li H, Tian L, Li Q, Luo J, Zhang Y. Analysis of the physicochemical properties of acaricides based on lipinski's rule of five. J Comput Biol. 2020;27(9):1397-406. doi: 10.1089/cmb.2019.0323, PMID 32031890.
31. Karatzas E, Zamora JE, Athanasiadis E, Dellis D, Cournia Z, Spyrou GM. ChemBioServer 2.0: an advanced web server for filtering, clustering and networking of chemical compounds, facilitating both drug discovery and repurposing. Bioinformatics. 2020;36(8):2602-4. doi: 10.1093/bioinformatics/btz976, PMID 31913451.
32. Athanasiadis E, Cournia Z, Spyrou G. ChemBioServer: a web-based pipeline for filtering, clustering and visualization of chemical compounds used in drug discovery. Bioinformatics. 2012;28(22):3002-3. doi: 10.1093/bioinformatics/bts551, PMID 22962344.
33. Dallakyan S, Olson AJ. Small-molecule library screening by docking with PyRx. Methods Mol Biol. 2015;1263:243-50. doi: 10.1007/978-1-4939-2269-7_19, PMID 25618350.
34. Yang H, Lou C, Sun L, Li J, Cai Y, Wang Z. AdmetSAR 2.0: web-service for prediction and optimization of chemical ADMET properties. Bioinformatics. 2019;35(6):1067-9. doi: 10.1093/bioinformatics/bty707, PMID 30165565.
35. Tutorial Huey R, Morris GM, Forli S, Wustl Edu. Using auto dock 4 and auto dock vina with auto dock tools: a tutorial; 2012.
36. O'Boyle NM, Banck M, James CA, Morley C, Vandermeersch T, Hutchison GR. Open Babel: an open chemical toolbox. J Cheminform. 2011;3(1):33. doi: 10.1186/1758-2946-3-33, PMID 21982300.
37. Wheeler G, Deng S, Toussaint N, Pushparajah K, Schnabel JA, Simpson JM. Virtual interaction and visualization of 3D medical imaging data with VTK and Unity. Healthc Technol Lett. 2018;5(5):148-53. doi: 10.1049/htl.2018.5064, PMID 30800321.
38. Gajula MNV, Kumar A, Ijaq J. Protocol for molecular dynamics simulations of proteins. Bio-Protocol. 2016;6(23). doi: 10.21769/BioProtoc.2051.
39. Bhowmik R, Roy S, Sengupta S, Sharma S. Biocomputational and pharmacological analysis of phytochemicals from Zingiber officinale (ginger), Allium sativum (garlic), and Murrayakoenigii (curry leaf) in contrast to type 2-diabetes. Int J App Pharm. 2021;13(5):280-6. doi: 10.22159/ijap.2021v13i5.42294.
40. Lopez Blanco JR, Aliaga JI, Quintana Orti ES, Chacon P. iMODS: internal coordinates normal mode analysis server. Nucleic Acids Res. 2014;42:W271-6. doi: 10.1093/nar/gku339, PMID 24771341.
41. Bauer JA, Pavlovic J, Bauerova Hlinkova V. Normal mode analysis as a routine part of a structural investigation. Molecules. 2019;24(18):3293. doi: 10.3390/molecules24183293, PMID 31510014.
42. Lopez Blanco JR, Ramirez E, Garcia S, Chacon P. Imods: fast exploration of macromolecular collective motions. Biophys J. 2014;106(2):653a, doi: 10.1016/j.bpj.2013.11.3614.
43. PubChem.nih.gov.1-(4-fluorophenyl)-N′-(4-methylphenyl)propane-1,3-diamine. Available from: https://pubchem.ncbi.nlm.nih.gov/compound/10038137.
44. Calıca Utku A, Budak G, Karabay O, Guclu E, Okan HD, Vatan A. Main symptoms in patients presenting in the COVID-19 period. Scott Med J. 2020;65(4):127-32. doi: 10.1177/0036933020949253, PMID 32807018.
45. Muller C, Hardt M, Schwudke D, Neuman BW, Pleschka S, Ziebuhr J. Inhibition of cytosolic phospholipase A2α impairs an early step of coronavirus replication in cell culture. J Virol. 2018;92(4). doi: 10.1128/JVI.01463-17, PMID 29167338.
46. Sanjeeva P, Rao BS, Ramana PV, Raju CN, Rajani V, Prasad VK. Synthesis, characterization and molecular docking studies of novel 2-(5- bromobenzofuran-2-yl)-5-substitutedphenyl-1,3,4-oxadiazole derivatives. J Adv Sci Res. 2021;12(3):61-8. doi: 10.55218/JASR.202112309.
47. Semih B, Tugce Nur Y, Mehmet Sinan D, Serdal K, Burhan T, Fevzi A. Tyrosine kinase inhibitors and COVID-19. J Oncol Pharm Pract. 2020;26(8):2072-3. doi: 10.1177/1078155220967081, PMID 33081581.
48. Roschewski M, Lionakis MS, Sharman JP, Roswarski J, Goy A, Monticelli MA. Inhibition of Bruton tyrosine kinase in patients with severe COVID-19. Sci Immunol. 2020;5(48):eabd0110. doi: 10.1126/sciimmunol.abd0110, PMID 32503877.
49. Bascı S, Ata N, Altuntas F, Yigenoglu TN, Dal MS, Korkmaz S. Outcome of COVID-19 in patients with chronic myeloid leukemia receiving tyrosine kinase inhibitors. J Oncol Pharm Pract. 2020;26(7):1676-82. doi: 10.1177/1078155220953198, PMID 32854573.
50. Krishnan P, Bastow KF. Novel mechanisms of DNA topoisomerase II inhibition by pyranonaphthoquinone derivatives-eleutherin, α lapachone, and β lapachone*. Biochem Pharmacol. 2000;60(9):1367-79. doi: 10.1016/s0006-2952(00)00437-8, PMID 11008131.
51. El-Kurdi B, Khatua B, Rood C, Snozek C, Cartin Ceba R, Singh VP. Mortality from coronavirus disease 2019 increases with unsaturated fat and may be reduced by early calcium and albumin supplementation. Gastroenterology. 2020;159(3):1015-1018.e4. doi: 10.1053/j.gastro.2020.05.057, PMID 32470338.